ACTA STEREOL 1995; 14/1: 5-16
STERMAT'94
ORIGINAL SCIENTIFIC PAPER

STEREOLOGICAL CHARACTERIZATION OF FIBRE DISPERSIONS IN CONCRETE

Piet Stroeven, Martijn Stroeven

Stevin Laboratory, Faculty of Civil Engineering, Delft University of Technology, Stevinweg 4, 2628 CN Delft, The Netherlands

ABSTRACT

Mechanical properties of fibre reinforced cementitious materials partly depend on the dispersion characteristics of the micro-reinforcement. Fibres of different materials and different sizes are employed. This paper concentrates on steel wire reinforcement. It deals with the methodology of determining experimentally global as well as local 3-D features. The mechanical model is designed on the basis of mechanisms of damage evolution derived from image analysis studies.

Key words: concrete, fibre, image analysis, computer-simulation, stereology.

INTRODUCTION

The production processes of fibre and wire reinforced cementitious materials will in general lead to partial orientation and segregation in the reinforcement structure. Since steel wire reinforced concrete is in civil engineering the most thoroughly investigated one among the micro-reinforced cementitious composites, this paper will particularly focus on this material. It is conventionally referred to as steel fibre (instead of wire) reinforced concrete (SFRC). The extent of partial orientation and segregation is well-documented for SFRC (Stroeven & Shah, 1978; Kasperkiewicz *et al*, 1978; Stroeven & Babut, 1986; Granju & Ringot, 1989; among others), so that data can be used as a reference.
Mechanical properties along the ascending branch of the stress-strain curve (eg. crack initiation strength, ultimate strength) have been shown to depend predominantly on *global* structural parameters. Hence, first order stereological concepts for quantitative image analysis can be employed for 3-D reconstruction of the fibre reinforcement structure. An overview of the methodological aspects of performing such a 3-D reconstruction will be given. The efficiency of the fibres is derived from the multitude of cracks in the plain cementitious body. Stiffness or crack initiation strength cannot be improved by the small fibre additions commonly employed in case of SFRC (say, 1 % by volume). The profit from the fibres is derived from the crack control capacity, leading to a moderate increase in ultimate strength and a dramatic improvement in toughness.
Post-ultimate behaviour is characterized by the formation of mesoscopic fracture process zones. The loading regime and the boundary conditions determine the number of such

zones. The fracture plane will ultimately be formed along the (curved) weakest chain link inside a fracture process zone of the fibre reinforced cementitious system (Stroeven & Shah, 1978). Under-reinforcement along the fracture surface can be quite considerable, particularly in materials research where relatively small specimens are used (Guo & Stroeven, 1989). Stress transfer over the fracture surface will depend on the efficiency of the fibre reinforcement (*local* number and orientation of the fibres bridging the fracture planes), and on the micromechanics involved (ie. the fibre pull-out characteristics). Stochastic and trigonometric factors are involved in this process. They govern the variation of global fibre density among potential fracture zones. They also determine the local structural features in the fracture process zone. This can be investigated by second order stereological methods, of which an approximate one will be introduced.

GLOBAL STEREOLOGICAL CONCEPT FOR IMAGE ANALYSIS IN SFRC

Access to the material body is provided by section and projection images. The following stereological relationships form the basis for assessment of the spatial characteristics of the fibre dispersion. In case of SECTIONS (figure 1)

$$L_V = 2\overline{P_A} \tag{1}$$

Total fibre length, L, per unit of volume, V $(L/V = L_V)$ is proportional to the average number of fibre intersections, P, per unit of sampled area, A, $(P/A = P_A)$. In case of PROJECTIONS (figure 2)

$$N_V = \frac{1}{t}(\overline{N'_A} - \frac{1}{2}L_V) \quad . \tag{2}$$

The number of fibres, N, per unit of volume is proportional to the average number of projected fibre parts, N', per unit of area. Slice thickness is t. Of course, $L_V = lN_V$, with l being fibre length in case of monosized fibres. In case of PROJECTIONS

$$L_V = \frac{2}{t}\overline{P'_L} \tag{3}$$

Total fibre length per unit of volume, L_V, is proportional to the average number of intersections, P', per unit of test line length, L. In this case the radiography image is

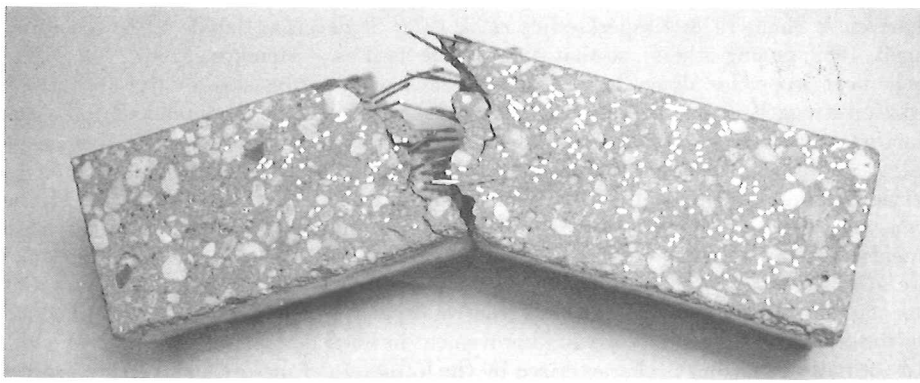

Fig. 1. Prismatic specimen sawn from larger SFRC element. Fibres are visible in the section plane and along the fracture area.

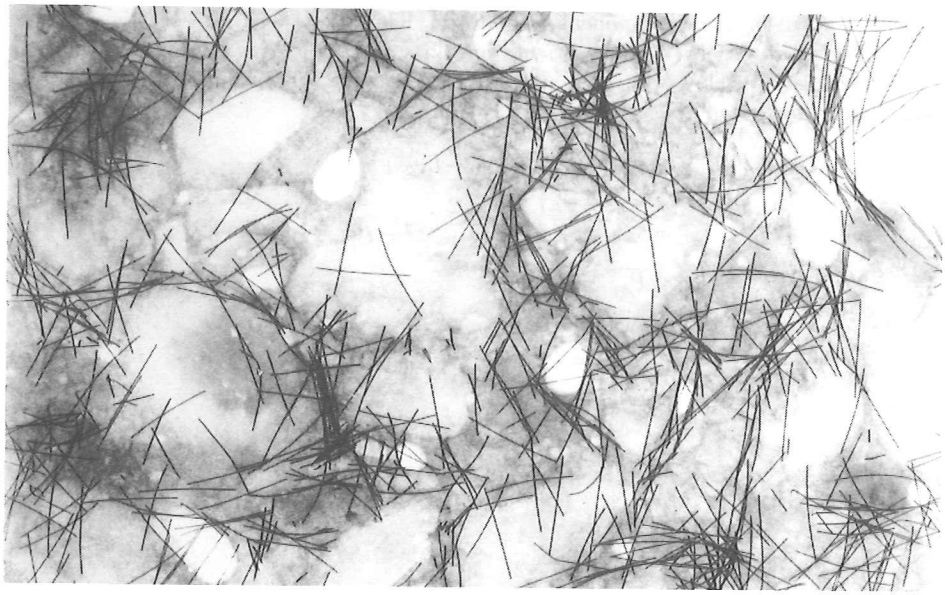

Fig. 2. X-ray radiography image of sawn SFRC slice revealing the larger particles and the steel fibre parts included in the slice.

covered by a line system with total length L, whereupon the number of intersections with the projected fibre parts are counted.

'Averaging' should be accomplished over randomly positioned and oriented samples. This is unpractical and expensive. Therefore, eqs (1) to (3) will be elaborated for a partially linear planar fibre structure, an approximation coming sufficiently close to the actual situation. For that purpose, a SFRC specimen is considered being compacted with its z-axis in the direction of the gravity field (hence, the $\{x, y\}$-plane corresponds to the orientation plane of the 2-D fibre component). The 1-D fibre portion will be oriented into the longitudinal direction of the specimen. The afore-mentioned formulas are also valid for 3-D fibre systems. The appropriate efficiency parameter is always 1/2. Hence,

$$\frac{1}{2}L_{V3} = P_A = \frac{P'_L}{t} = \frac{N'_A}{1 + \frac{2t}{l}} \tag{4}$$

The effective fibre length, $l/2$, equals the average projected length of the fibres along a line perpendicular to the section plane, alternatively, perpendicular to the projection plane (the X-ray image). This is obviously,

$$\overline{H_3} = \overline{l_{3proj}} = l\frac{\int_0^{\pi/2} \cos\theta \sin\theta \, d\theta}{\int_0^{\pi/2} \sin\theta \, d\theta} = \frac{1}{2}l \tag{5}$$

$\overline{H}$ is generally attributed as fibre tangent height. For the 2-D portion, the in-plane component of the tangent height amounts to

$$\overline{H_{2\|}} = l\frac{\int_0^{\pi/2} \cos\theta \, d\theta}{\int_0^{\pi/2} d\theta} = \frac{2}{\pi}l \tag{6}$$

whereas the out-of-plane component will be zero. Thus, $\overline{H_{2\perp}} = 0$.
$\overline{H_{1\|}}$ will equal fibre length in the orientation direction of the lineal fibre portion. This allows to specify eqs (1) to (3) for the partially linear planar fibre composite using *section*, respectively *projection* images (indicated by a prime)

$$\overline{P_{A_x}} = \frac{1}{2}L_{V3} + \frac{2}{\pi}L_{V2} + L_{V1} \tag{7}$$

$$\overline{P_{A_y}} = \frac{1}{2}L_{V3} + \frac{2}{\pi}L_{V2} \tag{8}$$

$$\overline{P_{A_z}} = \frac{1}{2}L_{V3} \tag{9}$$

$$\overline{N'_{A_x}} = \frac{t}{l}L_V + \frac{1}{2}L_{V3} + \frac{2}{\pi}L_{V2} + L_{V1} \tag{10}$$

$$\overline{N'_{A_y}} = \frac{t}{l}L_V + \frac{1}{2}L_{V3} + \frac{2}{\pi}L_{V2} \tag{11}$$

$$\overline{N'_{A_z}} = \frac{t}{l}L_V + \frac{1}{2}L_{V3} \tag{12}$$

$$\overline{P'_{L_x}}(0) = t(\frac{1}{2}L_{V3}) \tag{13}$$

$$\overline{P'_{L_x}}(\frac{\pi}{2}) = t(\frac{1}{2}L_{V3} + \frac{2}{\pi}L_{V2}) \tag{14}$$

$$\overline{P'_{L_y}}(0) = t(\frac{1}{2}L_{V3}) \tag{15}$$

$$\overline{P'_{L_y}}(\frac{\pi}{2}) = t(\frac{1}{2}L_{V3} + \frac{2}{\pi}L_{V2} + L_{V1}) \tag{16}$$

$$\overline{P'_{L_z}}(0) = t(\frac{1}{2}L_{V3} + \frac{2}{\pi}L_{V2}) \tag{17}$$

$$\overline{P'_{L_z}}(\frac{\pi}{2}) = t(\frac{1}{2}L_{V3} + \frac{2}{\pi}L_{V2} + L_{V1}) \tag{18}$$

Note that for $t \to 0$, eqs (10) to (12) transform into (7) to (9).
Determination of the three unknown fibre portions requires selecting three different relationships from eqs (7) to (18)! In a methodological sense the researcher is free to combine for that purpose the different experimental approaches. When X-ray equipment is not available sampling should be performed in the three Cartesian coordinate directions. The solution will be based on eqs (7) to (9). The effort of sawing can be reduced, however, by combining the experimental approaches in such a way, that sections and projection images are obtained of a single slice perpendicular to the longitudinal axis of the specimen. Use can be made of eqs (7), (13) and (14). This requires counting of fibres in the section plane and intersections in the projection plane. The superimposed line grid has to be positioned in two successive orthogonal directions. The analysis can be restricted to the radiography image by combining the directed secants approach with counting the number of fibre projections (in which case eq (10) is used).
The relevance of a global assessment of fibre structural characteristics is convincingly illustrated by data presented in the literature, such as in Stroeven (1979) and Donker (1986). Conventionally, the afore-mentioned framework is re-formulated in terms of fibre density, L_V, and degree's of fibre orientation, ω. The latter factors are defined by

$$\omega_{1,3} = \frac{L_{V1}}{L_V} \quad \text{and} \quad \omega_{2,3} = \frac{L_{V2}}{L_V}. \tag{19}$$

The resulting equations can be found in Stroeven & de Haan (1989) and Stroeven (1993). In addition to fibre anisometry fibres tend to segregate. This is of relevance for elements of SFRC subjected to bending. By analysing N_A over the height of sections (ie in the direction of the gravity field, Stroeven and Babut (1986) have quantified this structural parameter for various fibre densities. The presented stereological framework has also been used in this case.

DAMAGE EVOLUTION IN CONCRETE

On structural level fibre concrete can be conceived macroscopically heterogeneous. The largest particles can be up to three to six centimetres in diameter. The skeleton of cementitious materials is formed by densely packed particles of a wide range of sizes. The binding agent is the cement paste; bonding is generally relatively poor, however. In the unloaded situation the material contains as a result of shrinkage and other differential settlement effects myriads of small cracks, *particularly in the particle-matrix interface.* Additionally, residual stresses are built in on places where bond was not giving way. Upon loading, part of these stresses will easily lead to further crack initiation or to extension of existing cracks. Impact of this process of partial debonding of particle-matrix interfaces on stress-strain behaviour is small, so that the material is displaying linear elastic behaviour. Under load, a bond crack will tend to leave the interface layer at a certain angular extension; this will be stimulated when coalescence with nearest neighbours can take place in a favourable direction with respect to the global stress field. Degree of orientation of the damage structure will gradually grow revealing a prevailing orientation governed by the global stress field. An acceleration in crack coalescence will have a pronounced mechanical effect. The "discontinuity point" (DP) in the stress-strain curve represents this transition stage in damage evolution. In mechanical terms it is referred to as "crack initiation strength" or "onset of structural loosening" (Stroeven, 1973).
It is only beyond DP that crack propagation can be inhibited by the micro-reinforcement. "Ultimate strength" is associated with the bend over point (BOP) in the stress-strain curve. It cannot be related as easily to a typical stage in the process of structural loosening. Initially, crack coalescence will proceed in scattered regions, before gradually concentrating in so called "process zones", which will spread over the full width of the specimen's cross section with only a limited extension (in terms of particle size) in the orthogonal direction. Imposed global deformations will predominantly concentrate in the form of additional damage in these zones, reducing its load-bearing capacity: the specimen is yielding. A series of such zones will be formed parallel to the loading direction in compression. Spacing will be roughly equal to maximum grain size (Stroeven, 1973). In tension, a single fracture process zone will be formed.
Normally, volume percentages of the micro-reinforcement up to 1.5 to 2.0 are used. Only in SIFCON the fibre content will be much larger. The large number of coalescing cracks between particles in the stable loading range which determine BOP, is nevertheless effectively exploiting the micro-reinforcement. As a result, a moderate increase in BOP can be achieved. The mechanical model is based on this concept of a large number of locally reinforced mesocracks. Only the cracks unfavourably oriented with respect to the global stress field will have to be taken into consideration, of course. At a more advanced state of deformation, a much smaller number of macrocracks will govern the mechanical behaviour. Since they will be similarly oriented with respect to the global stress field, the same structural model can be employed.

MECHANICAL MODELLING OF SFRC

Opening up of cracks in matrix pockets causes fibres reinforcing these cracks to be partly pulled out and sheared over the crack edges (Brandt, 1985). The load transmitted perpendicularly to the crack surfaces by a single fibre enclosing an angle $(\frac{\pi}{2} - \theta)$ with the crack plane is

$$P_{f\perp} = \pi d\overline{l_i}\tau_f\,[\overline{\cos\theta} + f\,\overline{\sin\theta}] \tag{20}$$

with $\overline{l_i}$ being the average embedment length. f is the coefficient of friction. Anchoring facilities give rise to a 'concentrated force' at the end of the fibre, P'_f. The stress transferred perpendicular to the crack plane is for a 3-D dispersion given by, $\overline{\sigma}_{n3} = P_{f\perp} * \overline{N_{A3}}$, in which $\overline{N_{A3}} = \frac{1}{2}L_{V3}$. Eq (30) transforms into

$$\overline{\sigma}_{n3} = (P'_f + \frac{\pi}{4}dl\tau_f)\frac{1}{2}L_{V3}[\overline{\cos\theta} + f\,\overline{\sin\theta}] = \frac{1}{3}L_{V3}(1+f)(P'_f + \frac{\pi}{4}dl\tau_f) = \frac{1}{3}aV_{f3}\tau_f^* \tag{21}$$

with

$$\tau_f^* = (\tau_f + \tau'_f)(1+f) \tag{22}$$

in which a is the fibre aspect ratio and τ'_f is an equivalent friction resistance, calculated as the ratio of anchor load and average embedment length. P'_f will diminish in proportion to $\overline{N_{A3}}$ with growing crack opening, w. This equally holds for P_f, but this load is additionally reduced in proportion to the embedment length. Both reduction factors will amount to $(1-2\frac{w}{l})$. For $w \ll l$ the combined reduction factor will be $(1-2\frac{w}{l})^2 \cong (1-4\frac{w}{l})$. Herewith eq (21) can be written in the form

$$\overline{\sigma}_{n3} = \frac{1}{3}aV_{f3}(1+f)[(1-4\frac{w}{l})\tau_f + (1-2\frac{w}{l})\tau'_f] \tag{23}$$

In case $\tau'_f \ll \tau_f$ it is seen that $\overline{\sigma}_{n3}$ tends to zero for $w_u = l/4$, a value reported in the international literature. For significant values of τ'_f, $\overline{\sigma}_{n3}$ will tend to zero for larger values. However, τ_f will be reduced due to a polishing effect during early slippage, so that in experiments mostly lower values will be detected (see, eg, Stroeven, 1979).
The modelling concept for a 3-D fibre composite can also be defined for a 2-D one. The most relevant formula is

$$\overline{\sigma}_{n2\|} = (P'_f + \frac{\pi}{4}dl\tau_f)\frac{2}{\pi}L_{V2}(\frac{\pi}{4} + \frac{1}{2}f) \tag{24}$$

because

$$\overline{\cos\theta} = \frac{\int_0^{\frac{\pi}{2}}\cos^2\theta\,d\theta}{\int_0^{\frac{\pi}{2}}\cos\theta\,d\theta} = \frac{\pi}{4} \quad \text{and} \quad \overline{\sin\theta} = \frac{\int_0^{\frac{\pi}{2}}\cos\theta\sin\theta\,d\theta}{\int_0^{\frac{\pi}{2}}\cos\theta\,d\theta} = \frac{1}{2} \tag{25}$$

Operating as before eq (21) can be written in the form

$$\overline{\sigma}_{n2\|} = \frac{1}{2}aV_{f2}\tau_f^*\frac{1+\frac{2}{\pi}f}{1+f} = \frac{1}{2}aV_{f2}\tau_f^*C \tag{26}$$

with $C = (1 + 2f/\pi)/(1+f)$. Analogously,

$$\overline{\sigma}_{n1\|} = aV_{f1}\frac{\tau_f^*}{1+f} \tag{27}$$

For a *partially linear-planar fibre composite* ultimate tensile strength can be estimated as a consequence by

$$\overline{\sigma}_{nx} = (1 - V_f)\sigma_m + \frac{1}{3}aV_f\tau_f^*[1 + \frac{2-f}{1+f}\omega_{1,3} + \frac{1}{2(1+f)}\omega_{2,3}] \quad (28)$$

$$\overline{\sigma}_{ny} = (1 - V_f)\sigma_m + \frac{1}{3}aV_f\tau_f^*[1 - \omega_{1,3} + \frac{1}{2(1+f)}\omega_{2,3}] \quad (29)$$

$$\overline{\sigma}_{nz} = (1 - V_f)\sigma_m + \frac{1}{3}aV_f\tau_f^*[1 - \omega_{1,3} - \omega_{2,3}] \quad (30)$$

The early part of the descending branch can be modelled similarly as in case of the 3-D portion. The resulting formulas are for the most practical case of a *partially planar system*

$$\overline{\sigma}_{n\|} = (1 - V_f)\sigma_m(1 - \frac{w}{w_0}) + \frac{1}{3}aV_f\tau_f^*[1 + (\frac{3}{2}C - 1)\omega][1 - \frac{2w}{l}(\frac{2\tau_f + \tau_f'}{\tau_f + \tau_f'})] \quad (31)$$

$$\overline{\sigma}_{n\perp} = (1 - V_f)\sigma_m(1 - \frac{w}{w_0}) + \frac{1}{3}aV_f\tau_f^*[1 - \omega][1 - \frac{2w}{l}(\frac{2\tau_f + \tau_f'}{\tau_f + \tau_f'})] \quad (32)$$

in which w is the crack opening and w_0 its value at COP, where all additional deformations will accumulate in growing of the major crack. Stress transfer over the fracture plane will be zero for w_u-values between $l/2$ and $l/4$. w_u and w_0 differ two orders of magnitude, of course. This can be seen in figure 3, revealing stress-strain curves of SFRC in direct tension (Stroeven & Shah, 1978). Two different fibre types are added to the same cementitious matrix, ie. plain fibres (ie. $\tau_f' = 0$!) and hooked ones (for which τ_f' was dominant), the latter type being slightly longer (ie. 25 and 30 mm, respectively). Summarizing, in eq (31) C is a constant ($= (1 + \frac{2}{\pi}f)/(1 + f)$) only slightly deviating from unity. τ_f^* is defined by eq (22) and τ_f' equals the ratio of anchor load and average embedment length ($= l/4$). Eqs (28) to (30) present estimates of anisotropic ultimate strength values of a SFRC material with arbitrary fibre dispersion. Account is given to pull out and shearing of the fibres over the crack edges. Plain fibres and fibres with anchoring facilities are covered. For increasing crack openings, w, also the first (and most relevant) part of post-ultimate behaviour can be estimated (since the approximation holds for $w \ll l$).

SECOND ORDER STEREOLOGICAL APPROACH TO FIBRE DISPERSIONS

Along the length of specimens the fibre density was found to manifest a larger variation than could be explained on the basis of a 'natural' (Poisson-type of) dispersion of the fibres (Stroeven, 1979, and Donker, 1986). A computer-simulation study revealed significant contributions to scatter coming from the largest particles in the mix (Guo & Stroeven, 1989; Stroeven & Guo, 1989). This becomes at least qualitatively evident, seeing the disturbing effect of the large particles on fibre distribution in figure 2. Coalescing bond cracks will be confronted with local fibre reinforcement, density being of prime importance. Local features of the fibre dispersion cannot be obtained from first order stereological image analysis approaches. Such efforts will inevitably lead to subjective results (Granju & Ringot, 1989).

A second order approach for analysing fibre dispersions is described by Robine *et al* (1987) and by Hanisch *et al* (1985). The tools proposed for the analysis of *inner order* are the pair correlation function, $g(r)$, the radial distribution function, $R(r) = 4\pi\lambda r^2 g(r)$ and the integrated radial distribution function, $G(r) = \int_0^r 4\pi x^2 g(x)dx$. Herein, λ equals the line

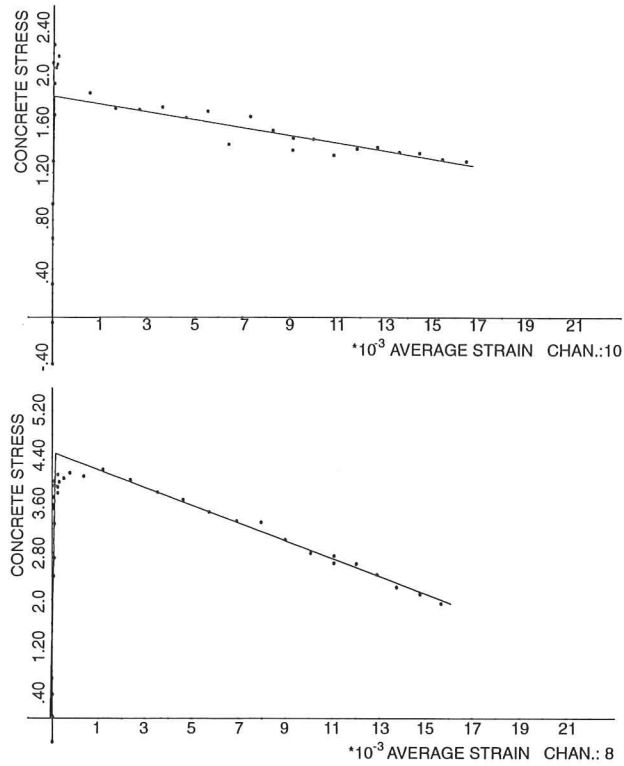

Fig. 3. Stress-strain curves of SFRC specimens in direct tension determined by clip gauges over the main crack; at the top, plain fibres are used, at the bottom hooked ones.

density, L_V. Most of the applied steel fibres are mono-sized slender elements (with an aspect ratio of up to 100) which can be treated properly as lineal elements in space.
$G(r)$ is for a Poisson line system given by

$$G(r) = 2r + \frac{4}{3}\pi r^3 L_V \tag{33}$$

$G(r)$ can be interpreted as the mean total fibre length of all fibre pieces inside a sphere with radius r located at a randomly chosen fibre centre. $G(r)$ can be estimated in case of the Poisson fibre system by a quantitative image analysis procedure. The procedure is illustrated in Stroeven & Stroeven (1991). A circular probe with radius r is successively positioned with its origin at all n centres, O_j, of the fibre intersections in the section plane ($j = 1, 2, 3...n$). The fibres should be at a distance r or more from the boundary. Define the distances of m fibre intersection enclosed by the circular probe to the horizontal axis through the origin of the circular probe by v_i (with $i = 0, 1...m(j)$). A function $G^*(r)$ can be calculated from observations in the section plane, ie. measurements of v_i. For moderate and large values of r, Hanisch *et al* (1985) have shown $G^*(r)$ to be an unbiased estimator of $G(r) - 2r$.
The following simple calculations have to be performed on the basis of the measurements

of v_i (see, also Stroeven & Stroeven, 1991):

$$V_j = 2\pi \sum_{i=0,1}^{m(j)} v_i \tag{34}$$

Hence, the recorded distances inside the circular probes are added, multiplied by 2π and thereupon averaged for all circle positions, n, by

$$G^*(r) = \frac{1}{n} \sum_{j=1,2}^{n} V_j \tag{35}$$

EXPERIMENTAL

The potentialities of such second order stereological techniques were assessed earlier on the basis of some of the roughly 300 section images, prepared from SFR mortar specimens tested by Babut and Stroeven (1985). To see how sensitive the second order approach was as to detecting differences in maximum grain size, a couple of additional specimens was prepared from a single, traditionally composed mix with a maximum grain size of 16 mm. For details, see Stroeven & Stroeven (1991).
Information on "inner order" is reflected by the differences between $G(r) - 2r = \tilde{G}(r)$ and $G^*(r)$. It is therefore convenient to plot the ratio of both curves: in the absence of particle influences a unit value would result. Figure 4 presents an example of such a curve derived from the fibre pattern shown at the left, representing a mortar (Stroeven & Stroeven, 1991). Fibre density in the matrix pockets is higher than bulk value. Coalescing interface cracks beyond discontinuity are as a consequence confronted with a relatively high fibre density. With growing 'level of the microstructure' fibre density will decline to a minimum value when the circular probe will also cover single particles. The dip in the curve can therefore be associated with 'particle size' as indicated in figure 4. This allows to distinguish between concrete and mortar mixes. Figure 5 presents one of the 2-D models of a simulated mono-sized particle-fibre composite. The structure (either 2-D or 3-D) is in a sort of Brownian movement. The picture therefore represents a state at a certain time. Such pictures are used to verify the experimentally observed phenomena. This allowed to systematically assess the influences exerted by different structural parameters like particle density and particle size. A relative minimum is approximately found for a probe radius equal to particle diameter, $r = d$. This dip in the curve becomes more pronounced the larger the number of particles per unit of volume. In the absence of particles (ie. for a very fine grained material) a constant unit value was found of $\tilde{G}(r)/G^*(r)$. Successive grain sizes exert their distinct influence - widening the minimum in the curve - provided particle density is large enough. For a concrete, the range of particle sizes exerting influence on the curve is (much) larger than in case of mortar. Hence, the dip in the experimental curve for mortar, shown in figure 4, will be so much widened for concrete that it cannot be distinguised from the rest of the curve. This is experimentally confirmed (Stroeven & Stroeven, 1991).

CONCLUSIONS

The presented methodological first order stereological framework allows an economic and reliable solution to the assessment of global fibre dispersion characteristics. The most

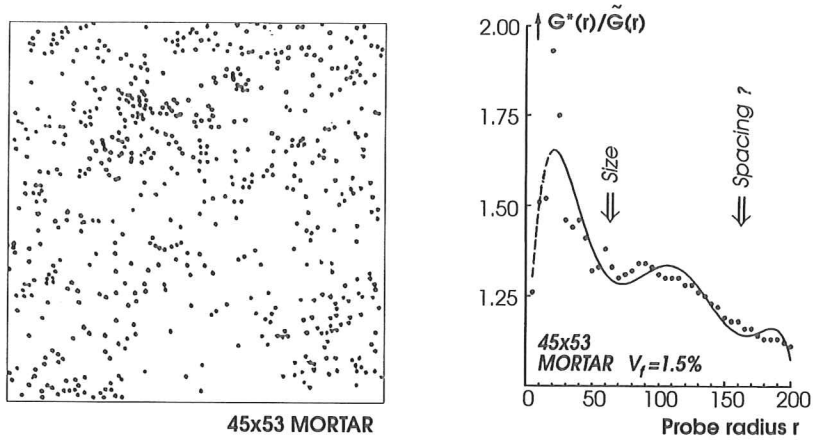

Fig. 4. Data pertaining to SFR mortar reflecting degrees of inner order in fibre dispersion.

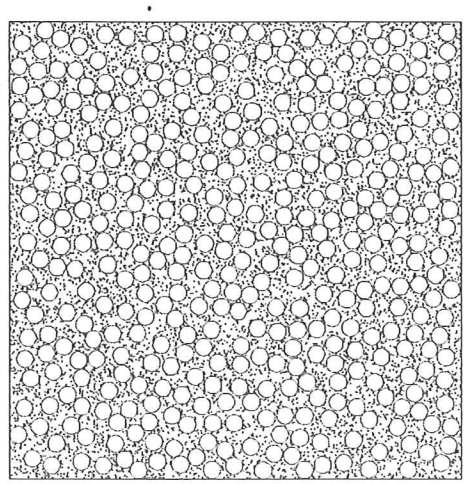

Fig. 5. Computer-simulated 2-D structure of a mono-sized particle-fibre structure. Diameter and areal fraction of the fibres are respectively 4 units and 0.02, and of the particles 80 units and 0.45.

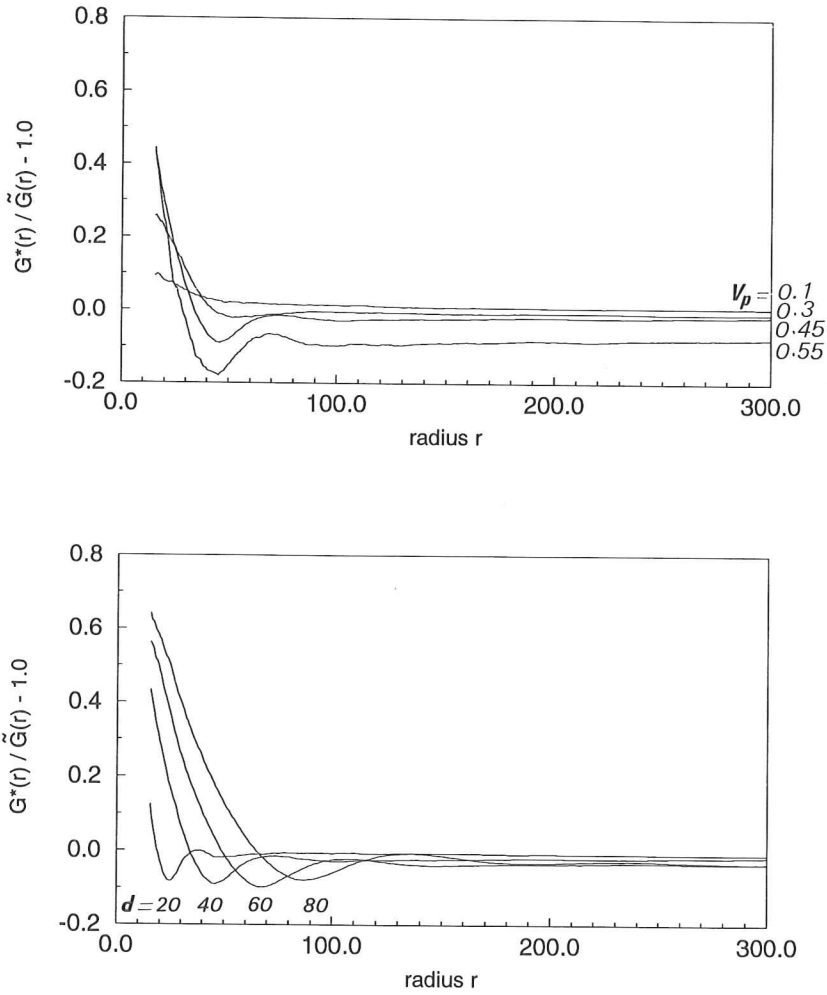

Figure 6. Application of second order stereological approach to fibre dispersion in computer-simulated SFRC; from top to bottom are shown: influence of volume fraction of a mono-sized particle system, V_p, on 'inner order' of the fibre system; the effect of grain size, d, on the local properties of the fibre distribution.

common situation of a partially linear-planar system can be described. Also segregation and boundary effects can be analysed in this way. Herewith, relevant mechanical properties (particularly anisotropic ultimate strength values) can be estimated. The study of local crack development (such as in fracture mechanics) and the modelling of the mechanical behaviour during yielding would require information on 'inner order' of the fibre dispersion. A second order stereological approach to this problem is outlined. The method indeed reveals characteristic influences of particles on fibre density as a function of the level of the microstructure.

REFERENCES

Brandt AM. The optimization of fibre orientation in brittle matrix composite materials. Report Stevin Laboratory, Delft University of Technology, 1985.

Donker L. Bending and splitting strength of steel fibre reinforced concrete plates, B-1: image analysis results. Fac Civ Engr Rep 1-68-3.: Delft Univ Techn, 1986 (in Dutch).

Granju JL, Ringot E. Amorphous iron reinforced concretes and mortars, comparison of the fibre arrangement. Acta Stereol 1989; 8/2: 689-94.

Guo W, Stroeven P. The analysis of wire distributions in computer-simulated wire reinforced materials. Spec Iss Acta Stereol 1989; 8/2: 683-8.

Kasperkiewicz J, Malmberg B, Skarendahl A. Determination of fibre content, distribution and orientation in steel fibre concrete by X-ray technique. In: Swamy RN, ed. Testing and test methods of fibre cement composites. Lancaster: Construction Press, 1978: 298-305.

Hanisch KH, König D, Stoyan D. The pair correlation function for point and fibre systems and its determination by planar sections. J Microsc 1985; 140: 361-70.

Robine H, Jernot J-P, Chermant J-L. Stereological determination of the radial distribution function of spheres. Acta Stereol 1987; 6/III: 159-64.

Stroeven P. Some aspects of the micromechanics of concrete. PhD thesis, Delft Univ Techn. 1973.

Stroeven P. Fibre concrete. Heron 1979; 24/4: 7-40.

Stroeven P. Structural characterization of steel fibre reinforced concrete. In: Brandt AM, Marshall IH, eds. Brittle matrix Composites 2. London: Elsevier Appl Sc, 1989: 34-43.

Stroeven P. Some global aspects of fibre reinforcement efficiency in concrete. In: Advanced technology on design and fabrication of composite materials and structures. Int Conf Torino May 24-28, 1993 (in print).

Stroeven P, Babut R. Fracture mechanics and structural aspects of concrete. Heron 1986; 31/2: 15-44.

Stroeven P, Guo W. Structural modelling and mechanical behaviour of steel fibre reinforced concrete. In: Barr B, ed. Fibre reinforced cements and concretes; recent developments. London: Elsevier Appl Sc, 1989: 345-54.

Stroeven P, Shah SP. Use of radiography-image analysis for steel fibre concrete. In: Swamy RN, ed. Testing and test methods of fibre cement composites. Lancaster: Construction Press, 1978: 345-53.

Stroeven P, Stroeven, M. Application of second order stereological method to steel wire reinforced concrete. Acta Stereol 1991; 11/1: 605-10.